Helm JL, Billam TP, Rakonjac A, Cornish SL, Gardiner SA.

Spin-Orbit-Coupled Interferometry with Ring-Trapped Bose-Einstein Condensates.

***Physical Review Letters* 2018, 120(6), 063201.**

Spin-Orbit-Coupled Interferometry with Ring-Trapped Bose-Einstein Condensates

J. L. Helm,[1] T. P. Billam,[2] A. Rakonjac,[3] S. L. Cornish,[3] and S. A. Gardiner[3]
[1]The Dodd–Walls Centre for Photonic and Quantum Technologies, Department of Physics, University of Otago, Dunedin 9016, New Zealand
[2]Joint Quantum Center (JQC) Durham–Newcastle, School of Mathematics, Statistics and Physics, Newcastle University, Newcastle upon Tyne NE1 7RU, United Kingdom
[3]Joint Quantum Center (JQC) Durham–Newcastle, Department of Physics, Durham University, Durham DH1 3LE, United Kingdom

(Received 10 January 2017; published 6 February 2018)

We propose a method of atom interferometry using a spinor Bose-Einstein condensate with a time-varying magnetic field acting as a coherent beam splitter. Our protocol creates long-lived superpositional counterflow states, which are of fundamental interest and can be made sensitive to both the Sagnac effect and magnetic fields on the sub-μG scale. We split a ring-trapped condensate, initially in the $m_f = 0$ hyperfine state, into superpositions of internal $m_f = \pm 1$ states and condensate superflow, which are spin-orbit coupled. After interrogation, the relative phase accumulation can be inferred from a population transfer to the $m_f = \pm 1$ states. The counterflow generation protocol is adiabatically deterministic and does not rely on coupling to additional optical fields or mechanical stirring techniques. Our protocol can maximize the classical Fisher information for any rotation, magnetic field, or interrogation time and so has the maximum sensitivity available to uncorrelated particles. Precision can increase with the interrogation time and so is limited only by the lifetime of the condensate.

DOI: 10.1103/PhysRevLett.120.063201

The endeavor to optimally apply matter-wave interferometry has generated many proposals and prototypes for ultrasensitive rotational [1–6], gravitational, or inertial [7–14] and gravity-wave [15–17] detection protocols. In parallel, optical confinement potentials allow the simultaneous trapping of atoms in different magnetic sublevels, constituting a spinor condensate [18–21]. In addition to their coherent nature, the ability to precisely manipulate motional and spin degrees of freedom using optical, radio-frequency, and magnetic fields makes spinor condensates a good candidate for the construction of an interferometer. We focus on a common path interferometric protocol, applying it to rotational sensing via Sagnac interferometry (where we note that our general common-path method is also applicable to zero-area Sagnac interferometry [22,23], an often discussed alternative to the Michelson geometry for optical gravity-wave detection [24–27]).

In this Letter, we propose a method of matter-wave interferometry in which a repulsively interacting spinor Bose-Einstein condensate (BEC) is split into a superpositional counterflow state [28,29] through the use of topological vortex imprinting [20,21,30–33], where the texture of an externally applied time-varying magnetic field (B field) is embedded in the condensate's spin and, hence, its phase. In the counterflow state, each atom is in a superposition of both spin and superflow, simultaneously moving clockwise and counterclockwise, while also occupying multiple hyperfine sublevels. This class of states is also of fundamental interest in that it yields superfluid-superfluid counterflow where the complicating effects of density gradients are substantially reduced [34]. As the spin and angular-momentum degrees of freedom are linked, they can be said to be spin-orbit coupled, and we refer to the method as spin-orbit-coupled interferometry (SOCI). This method is comparable to that proposed by Halkyard, Jones, and Gardiner [3] and has similarly maximized classical Fisher information (denoted F_C) [35]. The procedure uses experimentally accessible time-varying B fields as a "beam splitter" (Fig. 1). The "arms" of the interferometer are not spatially separate, constituting a common-path interferometer insensitive to a variety of perturbing factors due to its intrinsic symmetry. Advantages of our SOCI method are that (i) our interferometer can maximize F_C and so is shown to have the highest sensitivity achievable in the absence of entanglement; (ii) the symmetry and common-path geometry preclude many systematic phase aberrations; (iii) only standard magnetic fields are required for beam splitting, with no optical phase imprinting [28,29], mechanical stirring, or weak link [36–38] required; and (iv) the precision of our interferometer is limited only by the lifetime of the condensate.

We present our SOCI method analytically in the context of an idealized measurement and show that it converts an accumulated phase difference (due to rotation at angular frequency Ω, for example) between the counterflowing components into a difference among the populations, n_i, of the spin states. The measurement sensitivity of such a method can quantified by the classical Fisher information $F_C = \sum_i (\partial_\Omega n_i)^2 / n_i$ [35]. Using fully 3D numerical

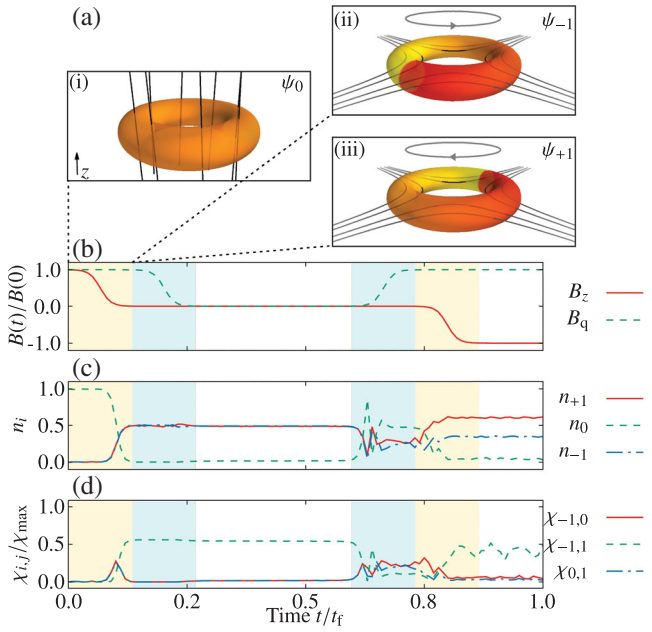

FIG. 1. Overview of spin-orbit-coupled interferometry. (a) Simulation isosurface plots at 0.2 of the peak density for the initial condition [$|0\rangle$ in (i)] and immediately after beam splitting [$|\mp 1\rangle$ in (ii) and (iii), respectively]. The color of the isosurface maps the phase, showing counterflow. Black curves show B-field lines. (b) B-field ramping scheme. Yellow (outer) shaded regions highlight the beam-splitting processes, while blue (inner) shaded regions show the phase unpinning processes. Numerically calculated norms $n_i = \int |\Psi_i|^2 d\boldsymbol{r}$ (c) and overlaps $\chi_{i,j}(t) = \int |\Psi_i|^2 |\Psi_j|^2 d\boldsymbol{r}$ (d) of the spinor components in the z-quantized basis are shown for a $\delta_S = \pi$ interferometry run ending at time t_f.

simulations of the spinor mean field, for experimentally realistic parameters, we show that our method maximizes F_C in the sense that F_C can be made equal to the maximum quantum Fisher information F_Q achievable for uncorrelated particles [35].

We treat a spin-F condensate as a system of $2F+1$ coupled BECs, working only in the z-quantized (ZQ) representation, where all spin states are labeled with reference to the z axis. The vector-valued order parameter is $\boldsymbol{\Psi} = \sum_{j=-1}^{1} \Psi_j |j\rangle$, where $F_z|j\rangle = j|j\rangle$, and $\hbar F_z/2$ is the z-direction angular-momentum operator in the ZQ basis. To consider the effect of rotations, we introduce an angular-momentum term [39,40] characterized by the angular velocity vector $\boldsymbol{\Omega}$; our full mean-field dynamical equations are then [20,21]

$$i\hbar \frac{\partial}{\partial t}\Psi_j = \left[-\frac{\hbar^2}{2m}\nabla^2 + V - i\hbar(\boldsymbol{r}\times\boldsymbol{\Omega})\cdot\boldsymbol{\nabla} + g_n \boldsymbol{\Psi}^\dagger\boldsymbol{\Psi}\right]\Psi_j + \{[g_s \bar{\mathbf{F}}\cdot\mathbf{F} - \mu_B g_F \mathbf{B}\cdot\mathbf{F}]\boldsymbol{\Psi}\}_j, \quad (1)$$

where the local spin vector $\bar{\mathbf{F}}$ has components $\bar{F}_\alpha = \Sigma_{j,k}\Psi_k^* \Psi_j \langle k|F_\alpha|j\rangle$. Here we have atomic mass m, Bohr magneton μ_B, and hyperfine gyromagnetic ratio g_F ($= -1/2$ for ^{87}Rb in the $F = 1$ manifold). The scattering terms are the normal interaction strength g_n and spin-spin interaction strength g_s [20]. The $V = m\omega_\perp^2[(\rho - R_0)^2 + z^2]/2$ term describes an optical ring trap [41], where $\rho = \sqrt{x^2+y^2}$, giving a radial trapping frequency $\omega_\perp$ and major radius R_0. While we restrict our analysis to this specific potential, we note that a more general toroidal potential (with density zero at $\rho = 0$) could be used to realize a similar interferometer. Gravity is taken to act in the z direction and does not alter the symmetry, and so we do not consider it further. In our numerics, we consider experimental parameters comparable to those described in Refs. [42,43]; however, for faster numerics, we take the radial trapping frequency to be $\omega_\perp = 2\pi \times 80$ Hz, the major radius of the ring to be $R_0 = 5a_\perp = 6.02$ μm, and the number of ^{87}Rb atoms to be $N = 10^4$.

The idealized behavior of the system can be understood through the eigenvectors of the $\mathbf{B}\cdot\mathbf{F}$ operator, in turn determined by the texture of the magnetic field. Our fundamental requirement is that the B field should have a nontrivial topology, such that a curve encircling the origin has a nonzero winding number, which is satisfied by either an anti-Helmholtz or Ioffe-Pritchard (IP) coil configuration. We consider the geometrically simpler IP configuration, which is quadrupolar in the x-y plane. The Cartesian components can then be written using cylindrical coordinates $\{\rho, \phi, z\}$ as $\mathbf{B}_{\mathrm{IP}} = (B_q(\rho)\cos(\phi), -B_q(\rho)\sin(\phi), B_z)$, where the quadrupolar field $B_q(\rho) = b'\rho$ varies linearly with ρ and the z-bias field is spatially uniform. For $F = 1$, in matrix representation $|1\rangle = (1,0,0)^T$, $|0\rangle = (0,1,0)^T$, and $|-1\rangle = (0,0,1)^T$:

$$\mathbf{B}\cdot\mathbf{F} = \begin{pmatrix} B_z & B_q e^{i\phi}/\sqrt{2} & 0 \\ B_q e^{-i\phi}/\sqrt{2} & 0 & B_q e^{i\phi}/\sqrt{2} \\ 0 & B_q e^{-i\phi}/\sqrt{2} & -B_z \end{pmatrix}. \quad (2)$$

The (spatially dependent) eigenvectors of Eq. (2) are

$$|\pm B\rangle = ([B \pm B_z]e^{i\phi}, \pm\sqrt{2}B_q, [B \mp B_z]e^{-i\phi})^T/2B, \quad (3)$$

$$|Z\rangle = (-B_q e^{i\phi}, \sqrt{2}B_z, B_q e^{-i\phi})^T/\sqrt{2}B, \quad (4)$$

where $B = (B_q^2 + B_z^2)^{1/2}$. The $|+B\rangle$ and $|-B\rangle$ eigenvectors denote the strong- and weak-field-seeking states with eigenvalues $\pm B$, while $|Z\rangle$ is field insensitive with eigenvalue 0. Through these eigenvectors, we can see the imprinting technique of Ref. [30]; varying B_q (via b') and B_z over time, the condensate remains in a given eigenvector of $\mathbf{B}\cdot\mathbf{F}$ but transfers between the m_f states, accumulating $l = F = 1$ quantum of angular momentum. Some radial dynamics can occur as the B field evolves, but these analytically separate out from the behavior described by $\mathbf{B}\cdot\mathbf{F}$ [30] and so are not addressed by our analytics. This implication of spin-gauge symmetry is confirmed by the full 3D numerics.

To achieve the counterflow state, we must first prepare our condensate in the $|0\rangle$ spin state with a large z-bias field $|B_z| \gg |B_q(R_0)|$. This constitutes the $|Z\rangle$ state. The $|0\rangle$ initial state can be achieved through rf pumping a $|-1\rangle$ (weak-field-seeking) condensate [44], following a transfer to an optical trap, where magnetic trapping is no longer required. With the initial condition fixed in the $|Z\rangle$ state, we obtain the counterflow state by ramping $|B_z|$ down to zero over a period T_s (Fig. 1) splitting the condensate into a superposition of spin up and spin down [see Eq. (4)]. We numerically explore two parameter regimes: (i) The quadrupolar field is characterized by an initial gradient $b' = 3.7$ G/cm, while the initial z-bias field is set to $B_z = 50$ mG (Fig. 1) (these parameters are consistent with Ref. [43]); (ii) we increase the field strengths by a factor of 10 to separate the Zeeman and nonlinear time scales, producing a smoother response curve (Fig. 2). We select the ramp-down period $T_s = 32$ ms (or 3.2 ms for the stronger B-field numerics) to be 50 times the Larmor precession time $T_L = 2\pi\hbar/(\mu_B g_F b' R_0) = 0.64$ ms (0.064 ms for the stronger B-field numerics), ensuring that the spins follow the B field adiabatically. The stronger fields are generally easier to generate experimentally and are easier to vary adiabatically due to their faster associated time scale, putting less stringent requirements on the level of field control. As the atoms in a given spin state have an associated flow field, the condensate is now in a superpositional counterflow state. During counterflow, the system is still described by the $|Z\rangle$ eigenstate, and so if we now return B_z to its initial value (or any other value of suitably large magnitude), the entire condensate will return to $|0\rangle$. We use this method for recombination in our interferometry protocol.

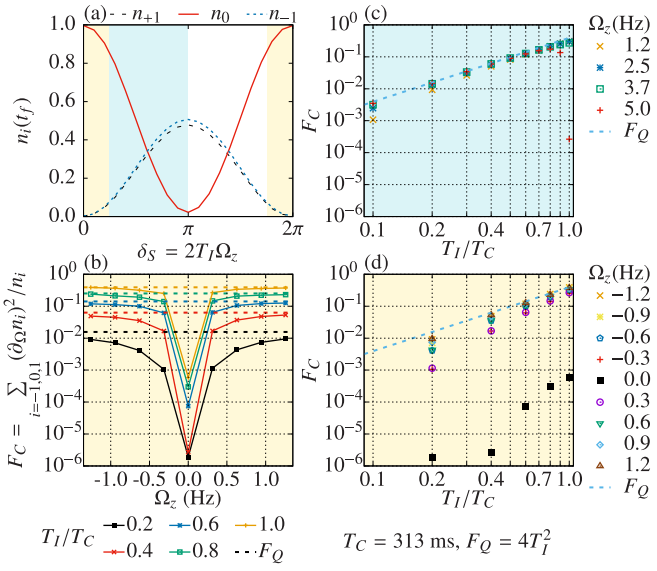

FIG. 2. Results of full 3D numerical simulations quantifying the performance of interferometry. (a) Response of the final norm in each component, $n_i(t_f)$, to varying Ω_z. These curves match our analytical result. (b)–(d) Comparison of quantum (F_Q) and classical (F_C) Fisher information. (b),(d) Readings made near the response curve turning point $\Omega_z = 0$ (yellow shading) have suppressed sensitivity ($F_C < F_Q$). (c) Readings made on linear segments of the response curve (blue shading) have the maximum sensitivity possible for uncorrelated states ($F_C = F_Q$). In all cases, we considered $N = 10^4$ ^{87}Rb atoms, with quadrupolar field gradient $b' = 37$ G cm^{-1}, initial z-bias field $B_z = 500$ mG, and field ramping time $T_s = 3.2$ ms.

With our beam-splitting and recombination protocols established, we can now consider the impact of a relative phase shift, consistent with the approach described in Ref. [3]. Artificially imprinting a relative phase difference δ between the spin-up and spin-down components after the split (at some time when $B_z = 0$), we can rewrite our counterflow state as a combination of all three eigenstates of $\mathbf{B}\cdot\mathbf{F}$:

$$|\Psi\rangle = \frac{1}{\sqrt{2}}(-e^{i(\phi+\delta/2)}, 0, e^{-i(\phi+\delta/2)})^T = \sqrt{\frac{1+\cos(\delta)}{2}}|Z\rangle - i\sqrt{\frac{1-\cos(\delta)}{2}}\left(\frac{|+B\rangle + |-B\rangle}{\sqrt{2}}\right). \tag{5}$$

Ramping B_z back up effects the recombination, after which the $|\pm B\rangle$ eigenvectors are the $|\pm 1\rangle$ states, while the $|Z\rangle$ eigenvector is the $|0\rangle$ state. Hence, projecting our final state onto the zero spin state via the $|0\rangle\langle 0|$ projector, we obtain an interferometric signal based on the condensate fraction in the $|0\rangle$ state, i.e., $\int |\Psi_0(t_f)|^2 d\boldsymbol{r} = [1+\cos(\delta)]/2$, where t_f is the time when our interferometry protocol ends. The populations of the different spin components can be observed experimentally by applying a field gradient in the z direction, resulting in Stern-Gerlach separation.

We now consider prospective interferometry applications, where Ω_z or B_z are nonzero during the interrogation counterflow period T_I. We assume the counterflow state is well described by Eq. (5), discarding structure and dynamics in the ρ and z directions; this assumption is validated by the numerical simulation. If we apply the $i\hbar(\boldsymbol{r}\times\boldsymbol{\Omega})\cdot\boldsymbol{\nabla}$ operator to each spin component of the counterflow state [Eq. (5)], this yields eigenvalues $\pm\hbar\Omega_z$ in the $|\pm 1\rangle$ components, respectively, and 0 in the $|0\rangle$ component. These eigenvalues can be incorporated into the diagonal elements of Eq. (2), combining the rotational and Zeeman terms of Eq. (1). The effect of the rotation is simply to offset the strength of the z-bias field, which is suppressed (enhanced) as the coordinate system rotates with (against) the magnetic dipole precession. This gauge transformation can be expressed as $\tilde{B}_z \to \tilde{B}_z + \tilde{\Omega}_z$, where $\tilde{\mathbf{B}} = \mu_B g_F \mathbf{B}/\hbar\omega_\perp$ and $\tilde{\boldsymbol{\Omega}} = \boldsymbol{\Omega}/\omega_\perp$ are dimensionless quantities. Experimentally, $\tilde{B}_z \gg \tilde{B}_q \gg \tilde{\Omega}_z$ is typically achievable (and implicit in considering the rotation to be a "small

effect"). Such a transformed system has analogous transformed eigenvectors. Hence, ramping down $|B_z| \to 0$, we are still in the $|Z\rangle$ eigenstate of $\mathbf{B}\cdot\mathbf{F}$ and therefore expect no accumulation of phase difference between the $|\pm 1\rangle$ components. In order to observe a relative phase accumulation, we must have a superpositional counterflow state in the absence of a quadrupolar field. Carefully ramping down B_q with $B_z = 0$ achieves this aim and unpins the phases of the counterflowing components, but if some small residual contribution $B_{zR} \neq 0$ remains, then the system may return to $|0\rangle$ over a slow B_q ramp down as dictated by Eq. (4), and counterflow is lost. To avoid this restorative effect, we must choose the ramp-down curve such that the B_q switch off is diabatic in some sense. For example, it could be smoothly decaying at first and then cut off instantaneously before the point where $B_q \approx 10 B_{zR}$ or be fully continuous but ramped over a suitably fast time scale. The key consideration should be reduction of the radial dynamics and heating associated with diabatic processes, noting that the smaller the residual field, the smaller the associated Zeeman energy, and so the less danger of heating. We also highlight that this restorative effect requires the residual field to satisfy $B_{zR} \ll B_q(R_0)$ ($\sim$1.57 mG for our weak B-field numerics). This upper bound scales linearly with R_0 and b' and can easily be raised. In the complete absence of magnetic fields (and, by spin-gauge symmetry, rotations), the hyperfine states become degenerate. In general, this leads to undesirable spin flips, which become more energetically allowable as $B \to 0$. Note that spin-flipping collisions are suppressed in the superpositional counterflow state [45]. Another possible source of undesirable spin flips is stray fields. However, assuming the field can be controlled on the milligauss scale, such processes have long associated time scales and can be ignored. Finally, we note that quantum and thermal fluctuations may be another source of spontaneous spin flips, but such an analysis is beyond the scope of this Letter. A strategy to avoid these spin flips would be to purposefully retain a nonzero B_{zR}.

Once the quadrupolar field is absent, the $|\pm 1\rangle$ components can evolve freely and accumulate a Sagnac phase δ_S for $\Omega_z \neq 0$ or a Zeeman-energy phase δ_Z for $B_{zR} \neq 0$. The phase magnitude can be quantified in terms of either the ring's enclosed area or the interrogation period T_I [3]. Allowing each component to perform the equivalent of one full circulation around the ring produces a Sagnac phase $\delta_S = 4A\Omega_z m/\hbar$ [3,4]. The particle velocity around the ring is given by a vortex velocity field $\mathbf{v} = (\hbar/m\rho)\hat{\boldsymbol{\phi}}$, and so the time for a single particle to fully circumnavigate the ring (such that $\rho = R_0$) to be $T_C = 2\pi R_0^2 m/\hbar = 2Am/\hbar$ ($= 313$ ms for our parameters). The phase accumulated for an arbitrary interrogation time T_I is then $\delta_S = (T_I/T_C)4\Omega_z Am/\hbar = 2\Omega_z T_I$. The same arguments apply for the Zeeman-energy phase under the substitution $\Omega_z \to (\mu_B/\hbar)B_z$. After interrogation, restoring the quadrupolar B field projects our phase-shifted wave function onto the eigenstates of $\mathbf{B}\cdot\mathbf{F}$. As phases are accumulated the populations in the $|\pm B\rangle$, the $|Z\rangle$ basis differs upon restoration of the quadrupolar field [Eq. (5)]. This induces some radial oscillations as the $|\pm B\rangle$ eigenstates are respectively strong- and weak-field seeking. These oscillations can be seen in the overlap integrals shown in Fig. 1(d); however, they do not affect the recombination as the radial dynamics analytically decouple from the eigenvectors of $\mathbf{B}\cdot\mathbf{F}$.

We show the results of numerical simulations of Eq. (1) (using CUDA [46]) in Figs. 1 and 2. In Fig. 1, we performed an interferometry procedure with Sagnac phase $\delta_S = \pi$, fixing the interrogation times $T_I = T_C$ for complete circulation around the ring and employing weak B fields consistent with Ray *et al.* [43]. These fields require longer time scales, allowing us to better see the dynamics. Figures 1(b), 1(c), and 1(d) display the full time evolution of the B field, the norms $n_i = \int |\Psi_i|^2 d\boldsymbol{r}$ of each component, and the density-density overlap integrals $\chi_{i,j}(t) = \int |\Psi_i|^2 |\Psi_j|^2 d\boldsymbol{r}$, respectively. There is a small difference between $n_{\pm 1}$ after recombination, as the weak fields used in these numerics make the Zeeman and nonlinear time scales comparable, compromising the dynamics. The result is still commensurate with our analytical predictions even in this suboptimal regime. We observe good overlap during the counterflow phase, verifying that radial dynamics do not affect the interrogation and that our method is a good example of a common-path interferometer. After restoring the quadrupolar field, oscillations are evident in the $\chi_{-1,+1}$ overlap integral as a result of the condensate now populating the field-sensitive $|\pm B\rangle$ eigenstates. In Fig. 2(a), we show the response curve obtained by varying Ω_z while again holding constant the interrogation time $T_I = T_C$. For these we used stronger B fields ($b' = 37$ G cm^{-1} and $B_z = 500$ mG). The response curve is smooth and in good quantitative agreement with our prediction [Eq. (5)]. We report that response curves obtained by varying B_{zR}, for field sensing on the sub-μG scale, are in good quantitative agreement with those obtained by varying Ω_z. In Figs. 2(b)–2(d), we show calculations of the classical Fisher information $F_C = \sum_{i=-1}^{1} (\partial_\Omega n_i)^2/n_i$ and show that for $\Omega_z \neq 0$ it is approximately equal to the quantum Fisher information $F_Q = 4l^2 T_I^2$, the upper limit achievable for uncorrelated particles and so the upper limit available to mean-field treatments [35]. The counterflow quantization is $l = F = 1$ in our method. This confirms that our SOCI protocol maximizes F_C for an arbitrary preselected read-off time.

For $\Omega \sim 0$ [Figs. 2(b) and 2(d)], the value of F_C is dominated by the small number count in the $|\pm 1\rangle$ modes such that even small deviations from zero are highly undesirable, as is the case with all two-mode interferometers. Our protocol can be designed to avoid this issue through the addition of an extra set of quadrupole bars to the IP coils. Using the secondary bars during recombination

allows an arbitrary rotation of the quadrupole field about the z axis, effecting a coordinate transformation equivalent to a phase shift δ [Eq. (5)]. Such a phase shift could move the response curve to a more favorable location with $F_C = F_Q$. In this way, any rotation could be measured with a precision limited only by the lifetime of the condensate. The sensitivity can be further increased by using a higher F manifold, increasing l, and increasing the precision. Note that the equivalency between $\tilde{\Omega}_z$ and $\tilde{B}_z$ requires that care be taken in experimental measurements. The maximum value of $\Omega_z = 2\pi \times 5.0$ Hz used in the numerics corresponds to $B_z = 3.56$ μG. As such, it should be straightforward to make single-shot field measurements on the sub-μG scale, as large rotations should be absent. Similarly, a spin-echo technique [47] would allow the exclusion of Zeeman phases [3].

In conclusion, we present a BEC interferometry protocol which requires only the careful control of standard B fields and an optical ring trap. Our protocol gives the greatest possible degree of access to measurement information for uncorrelated systems and, through its maximal spatial overlap, is a good candidate for Heisenberg limited interferometry [36,48,49]. We have also presented the results of full 3D multicomponent mean-field calculations of the Fisher information which demonstrate the robustness of our approach in the absence of idealizing approximations.

The data presented in this Letter can be found in Ref. [50].

We thank A. L. Marchant, R. J. Bettles, C. Weiss, and S. A. Haine for useful discussions, the United Kingdom Engineering and Physical Sciences Research Council (Grant No. EP/K03250X/1), and the Leverhulme Trust (Grant No. RP2013-K-009).

[1] A. Lenef, T. D. Hammond, E. T. Smith, M. S. Chapman, R. A. Rubenstein, and D. E. Pritchard, Phys. Rev. Lett. **78**, 760 (1997).
[2] T. L. Gustavson, P. Bouyer, and M. A. Kasevich, Phys. Rev. Lett. **78**, 2046 (1997).
[3] P. L. Halkyard, M. P. A. Jones, and S. A. Gardiner, Phys. Rev. A **81**, 061602 (2010).
[4] J. L. Helm, S. L. Cornish, and S. A. Gardiner, Phys. Rev. Lett. **114**, 134101 (2015).
[5] F. I. Moxley, J. P. Dowling, W. Dai, and T. Byrnes, Phys. Rev. A **93**, 053603 (2016).
[6] S. P. Nolan, J. Sabbatini, M. W. J. Bromley, M. J. Davis, and S. A. Haine, Phys. Rev. A **93**, 023616 (2016).
[7] M. J. Snadden, J. M. McGuirk, P. Bouyer, K. G. Haritos, and M. A. Kasevich, Phys. Rev. Lett. **81**, 971 (1998).
[8] A. Peters, K. Y. Chung, and S. Chu, Metrologia **38**, 25 (2001).
[9] J. M. McGuirk, G. T. Foster, J. B. Fixler, M. J. Snadden, and M. A. Kasevich, Phys. Rev. A **65**, 033608 (2002).
[10] S. Chu, A. Peters, and K. Y. Chung, Nature (London) **400**, 849 (1999).
[11] H. Müller, S.-w. Chiow, S. Herrmann, S. Chu, and K.-Y. Chung, Phys. Rev. Lett. **100**, 031101 (2008).
[12] H. Müller, A. Peters, and S. Chu, Nature (London) **463**, 926 (2010).
[13] P. A. Altin, M. T. Johnsson, V. Negnevitsky, G. R. Dennis, R. P. Anderson, J. E. Debs, S. S. Szigeti, K. S. Hardman, S. Bennetts, G. D. McDonald, L. D. Turner, J. D. Close, and N. P. Robins, New J. Phys. **15**, 023009 (2013).
[14] B. Canuel, F. Leduc, D. Holleville, A. Gauguet, J. Fils, A. Virdis, A. Clairon, N. Dimarcq, C. J. Bordé, A. Landragin, and P. Bouyer, Phys. Rev. Lett. **97**, 010402 (2006).
[15] G. M. Tino and F. Vetrano, Classical Quantum Gravity **24**, 2167 (2007).
[16] S. Dimopoulos, P. W. Graham, J. M. Hogan, M. A. Kasevich, and S. Rajendran, Phys. Rev. D **78**, 122002 (2008).
[17] P. W. Graham, J. M. Hogan, M. A. Kasevich, and S. Rajendran, Phys. Rev. D **94**, 104022 (2016).
[18] T.-L. Ho, Phys. Rev. Lett. **81**, 742 (1998).
[19] T. Ohmi and K. Machida, J. Phys. Soc. Jpn. **67**, 1822 (1998).
[20] D. M. Stamper-Kurn and M. Ueda, Rev. Mod. Phys. **85**, 1191 (2013).
[21] Y. Kawaguchi and M. Ueda, Phys. Rep. **520**, 253 (2012).
[22] K.-X. Sun, M. M. Fejer, E. Gustafson, and R. L. Byer, Phys. Rev. Lett. **76**, 3053 (1996).
[23] T. Eberle, S. Steinlechner, J. Bauchrowitz, V. Händchen, H. Vahlbruch, M. Mehmet, H. Müller-Ebhardt, and R. Schnabel, Phys. Rev. Lett. **104**, 251102 (2010).
[24] J. Mizuno, A. Rüdiger, R. Schilling, W. Winkler, and K. Danzmann, Opt. Commun. **138**, 383 (1997).
[25] M. Punturo *et al.*, Classical Quantum Gravity **27**, 084007 (2010).
[26] N. Mavalvala, D. E. McClelland, G. Mueller, D. H. Reitze, R. Schnabel, and B. Willke, Gen. Relativ. Gravit. **43**, 569 (2011).
[27] B. P. Abbott (LIGO Scientific Collaboration and Virgo Collaboration), Phys. Rev. Lett. **116**, 061102 (2016).
[28] S. Thanvanthri, K. T. Kapale, and J. P. Dowling, Phys. Rev. A **77**, 053825 (2008).
[29] K. T. Kapale and J. P. Dowling, Phys. Rev. Lett. **95**, 173601 (2005).
[30] T. Isoshima, M. Nakahara, T. Ohmi, and K. Machida, Phys. Rev. A **61**, 063610 (2000).
[31] S.-I. Ogawa, M. Möttönen, M. Nakahara, T. Ohmi, and H. Shimada, Phys. Rev. A **66**, 013617 (2002).
[32] Z. F. Xu, P. Zhang, R. Lü, and L. You, Phys. Rev. A **81**, 053619 (2010).
[33] J. Lovegrove, M. O. Borgh, and J. Ruostekoski, Phys. Rev. A **93**, 033633 (2016).
[34] C. Hamner, J. J. Chang, P. Engels, and M. A. Hoefer, Phys. Rev. Lett. **106**, 065302 (2011).
[35] S. A. Haine, Phys. Rev. Lett. **116**, 230404 (2016).
[36] S. Ragole and J. M. Taylor, Phys. Rev. Lett. **117**, 203002 (2016).
[37] S. Eckel, F. Jendrzejewski, A. Kumar, C. J. Lobb, and G. K. Campbell, Phys. Rev. X **4**, 031052 (2014).
[38] F. Jendrzejewski, S. Eckel, N. Murray, C. Lanier, M. Edwards, C. J. Lobb, and G. K. Campbell, Phys. Rev. Lett. **113**, 045305 (2014).
[39] A. Aftalion and Q. Du, Phys. Rev. A **64**, 063603 (2001).
[40] P. Mason and A. Aftalion, Phys. Rev. A **84**, 033611 (2011).

[41] T. A. Bell, J. A. P. Glidden, L. Humbert, M. W. J. Bromley, S. A. Haine, M. J. Davis, T. W. Neely, M. A. Baker, and H. Rubinsztein-Dunlop, New J. Phys. **18**, 035003 (2016).
[42] A. Rakonjac, A. L. Marchant, T. P. Billam, J. L. Helm, M. M. H. Yu, S. A. Gardiner, and S. L. Cornish, Phys. Rev. A **93**, 013607 (2016).
[43] M. W. Ray, E. Ruokokoski, S. Kandel, M. Möttönen, and D. S. Hall, Nature (London) **505**, 657 (2014).
[44] M.-S. Chang, C. D. Hamley, M. D. Barrett, J. A. Sauer, K. M. Fortier, W. Zhang, L. You, and M. S. Chapman, Phys. Rev. Lett. **92**, 140403 (2004).
[45] For the stated interaction strengths, our system is ferromagnetic ($g_s < 0$), and its energy is minimized for maximal $|\tilde{\mathbf{F}}|$. The splitting procedure generates a counterflow state for which $|\tilde{\mathbf{F}}| = 0$ and so minimizes the Hamiltonian energy of antiferromagnetic ($g_s > 0$) systems [18]. As such, the counterflow state constitutes a metastable excited state for ferromagnetic systems but would be a stable ground state for antiferromagnetic systems (e.g., ^{23}Na in $F = 1$ or ^{87}Rb in $F = 2$). However, since ^{87}Rb is only weakly ferromagnetic, the state's instability has a long associated time scale.
[46] J. Nickolls, I. Buck, M. Garland, and K. Skadron, Queueing Syst. Theory Appl. **6**, 40 (2008).
[47] E. L. Hahn, Phys. Rev. **80**, 580 (1950).
[48] C. Gross, J. Phys. B **45**, 103001 (2012).
[49] A. J. Ferris and M. J. Davis, New J. Phys. **12**, 055024 (2010).
[50] Durham University Collections, http://dx.doi.org/10.15128/r1m900nt41q.